Energy xxx (2015) 1–8

Contents lists available at ScienceDirect

Energy

journal homepage: www.elsevier.com/locate/energy

Impact of micromixing on performance of a membrane-based absorber

Rasool Nasr Isfahani, Sajjad Bigham, Mehdi Mortazavi, Xing Wei, Saeed Moghaddam*

Department of Mechanical and Aerospace Engineering, University of Florida, Gainesville, FL 32611, USA

ARTICLE INFO

Article history:
Received 21 January 2015
Received in revised form
3 August 2015
Accepted 5 August 2015
Available online xxx

Keywords:
Absorption refrigeration system
Membrane-based absorption
Lithium bromide (LiBr)
Micro-mixing

ABSTRACT

In this study, microstructures are employed to manipulate thermohydraulic characteristics of the lithium bromide (LiBr) solution flow in a membrane-based absorber in order to enhance the absorption rate. In a membrane-based absorber, the liquid absorbent is constrained between a solid wall and a highly permeable membrane, thus facilitating manipulation of the flow properties. Recent numerical studies have shown that transport mode in a laminar flow can be changed from diffusive to advective via the implementation of surface microstructures on the flow channel walls. Here, we experimentally evaluate the enhancement in absorption rate caused by the introduction of microstructures on the solution flow channel wall of a membrane-based absorber. The experiments are conducted in a fully instrumented membrane-based absorption refrigeration system. The geometry and dimensions of the microstructures are based on the optimal values determined in our previous numerical studies. Absorption rates as high as that of a 100-μm-thick solution film (in the absence of wall features) is achieved but at two orders of magnitude less pressure drop. The achievement of a high absorption rate at a relatively low solution pressure drop in the proposed approach enhances the prospect of developing large-scale membrane-based absorbers.

1. Introduction

ARS's (absorption refrigeration systems) can be an alternative for the common cooling and heating systems. However, in their current format, ARS's are not competitive with the existing VCS's (vapor compression systems) in residential and small commercial buildings sector due to their high initial cost and large volume per unit cooling capacity. The absorber heat exchanger is widely recognized as a component that greatly impacts the size, cost, and performance of ARS's. In a conventional falling film shell-and-tube absorber, the refrigerant (commonly water) vapor generated in the evaporator is absorbed into a solution (commonly lithium bromide, LiBr) sprayed over a tube bundle. Enhancing the absorption rate has been the subject of many studies [1–10] focused on advancing the falling film absorption technology. Isfahani and Moghaddam [3] provide an overview of these studies and conclude that, despite many efforts, substantial enhancement in the absorption rate has not been achieved due to the challenges of controlling thermohydraulic characteristics of a falling LiBr solution film.

Recently, utilization of membranes has been proposed to enhance the absorption rate [11–21] and to develop absorbers in new inherently compact forms such as the plate-and-frame heat exchanger configuration. Yu et al. [19] numerically studied absorption characteristics of the LiBr solution flow and concluded that heat and mass transfer limits in a LiBr solution flow could be improved, if the solution flow thickness is maintained within a few hundred microns while the flow velocity is increased. Implementation of a thin solution flow reduces the heat diffusion path to the cooling surface beneath the solution film, and increasing the solution flow velocity reduces the concentration boundary layer thickness. In a subsequent experimental study, Isfahani and Moghaddam [12] demonstrated that a thin layer of LiBr solution could be constrained between a superhydrophobic nanofibrous membrane and a solid wall, and its absorption characteristics could be manipulated through independent control of the flow thickness and velocity. In their approach, the water vapor permeates through the membrane and is subsequently absorbed into the LiBr solution. Their results confirmed that the absorption rate can be significantly enhanced when a solution film thickness on the order of 100 μm and highly porous membranes are implemented.

In a recent numerical study, Bigham et al. [22] reported further enhancement of the absorption process in a membrane-based

* Corresponding author.
E-mail address: saeedmog@ufl.edu (S. Moghaddam).

http://dx.doi.org/10.1016/j.energy.2015.08.006
0360-5442/

absorber through utilization of microstructures on the solution channel bottom wall. Such structures have been previously shown to induce mixing in an otherwise laminar flow in microchannels [23–26]. In a similar vein, confinement of the LiBr solution flow in a membrane-based absorber provides an opportunity to manipulate the microscale transport events within the solution film. A well-designed channel wall will induce vortical structures in the flow that continuously replenish the membrane-solution interface (where the absorption takes place) with fresh concentrated solution from the middle and bottom of the flow channel. This approach enhances the utility of the membrane-based technology for absorbers with larger capacities because a thicker solution film limits the solution flow pressure drop in a large absorber. In a laminar flow $\Delta P \propto \dot{m}_{sol}/D_h^3$ ($\dot{m}_{sol}$ is the solution flow rate and D_h is the channel hydraulic diameter). This means that increasing the channel hydraulic diameter by a factor of 5 (as discussed later in this paper) results in 125 times reduction in the solution pressure drop. Reducing the pressure drop eases the manifolding burden of the absorber.

Bigham et al. [22] employed the herringbone structures (hereafter called “ridges”) proposed by Strook et al. [26] to enhance mixing in microfluidic devices. The method involves generating chaotic advection within the flow through stretching and folding the laminar streamlines. Fig. 1 shows a computationally obtained streamline of the flow over the ridges. Evidently, the herringbone structures generate anisotropic resistance to the absorbent flow, which stretches and twists a portion of the absorbent flow volume.

In the following section, first, an overview of the numerical simulations (including governing equations and assumptions) illustrating physics of the micro-mixing process and optimal dimensions of the ridge structure is provided (further details are presented in Bigham et al.'s [22] study). Then, implementation of the optimal design into a membrane-based absorber and studies conducted to assess the absorber performance are presented. The effects of important parameters such as vapor pressure and cooling water temperature on the absorption rate are discussed.

2. Absorber design

The absorption process in a membrane-based absorber with a flat channel surface is diffusion-limited. To show this limitation, an in-house computational fluid dynamics solver based on LBM (lattice Boltzmann method) [27,28] which is verified in our prior publications [18,19,22] is evoked. Here, a brief overview of the modeling approach is provided. In a membrane-based absorber, the vapor has to pass through the membrane pores before reaching the LiBr solution. The numerical procedure consists of two steps. In the first step, a continuum-based approach is used to model heat and mass transport inside the solution. In the second step, to simulate the vapor flux through the membrane, Dusty-Gas model [29] is used, since the flow is in the transitional or free molecular flow regime [19]. According to the Dusty-Gas model [29], the mass transfer through a membrane consists of diffusion and viscous fluxes. The molar diffusion flux is given by:

$$N^D = D_e^k \frac{-1}{RT}\Delta p \tag{1}$$

$$D_e^k = \frac{2\varepsilon r}{3\tau}\sqrt{\frac{8RT}{\pi M}} \tag{2}$$

where R is the gas constant, M is the molecular weight, r is the pore radius, ε is the membrane porosity, and τ is the membrane tortuosity. The molar viscous flux is given by:

$$N^V = \frac{-p}{RT\mu}\frac{\varepsilon r^2}{8\tau}\Delta p \tag{3}$$

where μ is the viscosity and p is the pressure. The total mass flux through the membrane pores can be written as the sum of the diffusion and viscous fluxes:

$$N = N^D + N^V \tag{4}$$

The vapor mass flux through the membrane can be then computed from Ref. [19]:

$$J = k_m(p_v - p_i), \quad k_m = -\frac{M}{\delta_m}\left(\frac{D_e^k}{RT} + \frac{pB_0}{RT\mu}\right) \tag{5}$$

where k_m is the membrane mass transfer coefficient or permeability, p_v is the water vapor pressure, p_i is the water vapor pressure of the solution at the interface and δ_m is the membrane thickness.

At the membrane surface, it is supposed that the LiBr solution and the vapor are at an equilibrium state. The mass flux across the membrane compared to the mass flux along the channel as well as heat transferring to the vapor phase through the membrane are all assumed to be negligible. Therefore, at the membrane surface, the following heat and mass boundary conditions are used [7,19,30–32]:

$$k(T,X)\frac{\partial T}{\partial n} = h_{fg}(T,X)\cdot k_m(p_v - p_i(T,X)) \tag{6}$$

$$D(T,X)\cdot\rho(T,X)\frac{\partial X}{\partial n} = k_m(p_v - p_i(T,X)) \tag{7}$$

where h_{fg} is the latent heat of evaporation, ρ is the solution density, and n is the interface normal direction. The LiBr properties are provided by McNeely [33].

No-slip and no-flux boundary conditions are used for momentum and the concentration equations, respectively, at the cooling surface. A linear temperature distribution is used at the cooling surface. The temperature and concentration are specified at the inlet, while a zero gradient boundary condition was used for both the temperature and concentration at the outlet. Also, symmetric conditions are applied on the sides of the flow domain. The governing equations are summarized in Table 1.

To solve the governing equations with the mentioned boundary conditions, an in-house computational fluid dynamics solver based

Fig. 1. A 3D schematic of surface features at the floor of a microchannel (microchannel is not shown in the picture) and a fluid particle streamline.

Please cite this article in press as: Nasr Isfahani R, et al., Impact of micromixing on performance of a membrane-based absorber, Energy (2015), http://dx.doi.org/10.1016/j.energy.2015.08.006

Table 1
Governing equations and main boundary conditions.

Equation		Mathematical form	Comments
2.1	Momentum	$\rho\, u_j\, u_{i,j} = -p_{,i} + \mu\, u_{i,jj}$	μ is dynamic viscosity
2.2	Energy	$u_j\, T_{,j} = \alpha\, T_{,jj}$	α is thermal diffusivity
2.3	Concentration	$u_j\, X_{,j} = D\, X_{,jj}$	D is mass diffusivity

on the LBM (lattice Boltzmann method) and a finite difference method for the concentration and temperature fields are used. A detailed description of the code is provided in Yu and Ladd [27]. In the LBM, the fluid is simulated by fictive particles with a mass distribution function of $f(\vec{x}, \vec{e}, t)$. To predict the motion of these particles, the Boltzmann equation is solved over a discrete lattice mesh. The popular SRT (single relaxation time) model, with the time step δt and space step $e_\alpha\, \delta t$, is:

$$f_\alpha(X_i + e_\alpha \delta t, t + \delta t) - f_\alpha(X_i, t) = -\frac{1}{\lambda}\left[f_\alpha(X_i, t) - f_\alpha^{(eq)}(X_i, t)\right] \tag{8}$$

where e_α is the discrete particle velocity set, λ the normalized relaxation time, and X_i a point in the discretized physical space. Eq. (8) is in fact the discrete lattice Boltzmann equation [34] with BGK (Bhatnagar-Gross-Krook) approximation [35]. The viscosity in the N–S equation derived from Eq. (8) is:

$$\nu = \left(\lambda - \frac{1}{2}\right) c_s^2 \delta t \tag{9}$$

where C_s is the speed of sound. This choice of the viscosity makes formally the LBGK (Lattice-Bhatnagar-Gross-Krook) scheme a second order method for solving incompressible flows [28]. The positivity of the viscosity requires that $\lambda > 0.5$. In Eq. (8), $f_\alpha(X_i,t)$ is the discretized distribution function associated with the α-th discrete velocity e_α and $f_\alpha^{(eq)}$ is the corresponding equilibrium distribution function.

The macroscopic quantities (such as mass density ρ and momentum density $\rho\vec{u}$) can be obtained by evaluating the hydrodynamic moments of the distribution function f as follows:

$$\rho = \sum_\alpha f_\alpha^{eq} \tag{10}$$

$$\rho\vec{u} = \sum_\alpha f_\alpha^{eq}\vec{e}_\alpha \tag{11}$$

A grid independence study was performed to ensure that the computational results are independent of the grid size. The maximum error in the absorption rate was found to be less than 2% when the grid size was reduced by a factor of 2. For a detailed discussion about the solver, the numerical procedure and the numerical validation, the readers are referred to our prior publications [18,19,22].

A typical concentration contour in an absorber with a flat surface is provided in Fig. 2. As it can be seen, a thick concentration boundary layer is formed at the vapor–liquid interface. Bigham et al. [22] conducted a parametric study to determine the optimal ridge geometry for a membrane-based absorber. Through their simulation, they determined that the ridge height must be more than 50% of the main channel height to produce surface vortices with sufficient momentum to impact the main flow and continuously replenish the solution-membrane interface with a concentrated solution. In the parametric range of their study, for a channel with a height of 500 μm, they achieved the maximum absorption rate using 300-μm-tall and 250-μm-wide ridges that are spaced 300 μm apart and oriented 30° with respect to the fluid direction.

Stroock et al. [26] and Sundararajan and Stroock [36] showed that the microstructures essentially stimulate the heat and mass transfer rates by improving four transport processes: mixing, interfacial transfer, axial dispersion, and spatial sampling. Contribution of each individual transport process to the overall heat and mass transport rates is difficult to assess experimentally and beyond the scope of the present study. However, transverse velocity components generated by the transport processes could be used as an overall quantitative assessment. Fig. 3 shows the y and z components of the velocity vector along the microchannel at y = 180 μm and z = 750 μm (i.e. 50 μm below the vapor–liquid interface). The results clearly show that the microstructures generate transverse velocity components of up to 1.4 mm/s in the y-direction and 0.1 mm/s in the z-direction. The results also indicate a major difference (approximately 4–5 times) between the y component of the velocity on the long and short ridges. The maximum transverse velocity in the y direction occurs on the long arm of the ridges and the average value of the y-velocity is 1.4 mm/s, which is 12% of the x component of the velocity. To elucidate how these ridges affect the flow thermohydraulic characteristics, typical iso-concentration surfaces within the bulk flow are provided in Fig. 4a. A set of flow cross-sectional views depicting the solution mixing process is provided in Fig. 4b. As shown, the ridges induce vortices within the solution film, which continuously bring concentrated solution from the bottom and middle of the solution channel to the vapor–liquid interface where absorption occurs. These vortices interrupt the concentration boundary layer growth and lead to enhancement in the absorption rate, as demonstrated experimentally in the following section.

3. Experiment

3.1. Test article

A photograph of the absorber heat exchanger along with 3D drawings showing the wall structures dimensions are provided in Fig. 5. The overall dimensions of the absorber are 311 × 117 mm^2 with an active area of 195 × 38 mm^2. The solution microchannels and ridges are machined within the active area. The solution is

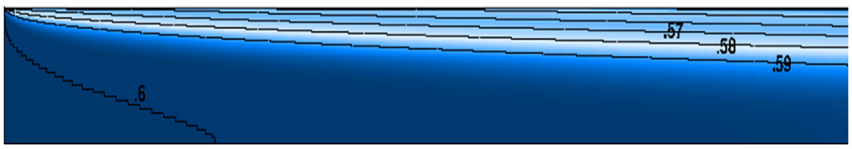

Fig. 2. LiBr solution concentration contours within a 500-micron-thick and 600-mm-long flow channel.

Please cite this article in press as: Nasr Isfahani R, et al., Impact of micromixing on performance of a membrane-based absorber, Energy (2015), http://dx.doi.org/10.1016/j.energy.2015.08.006

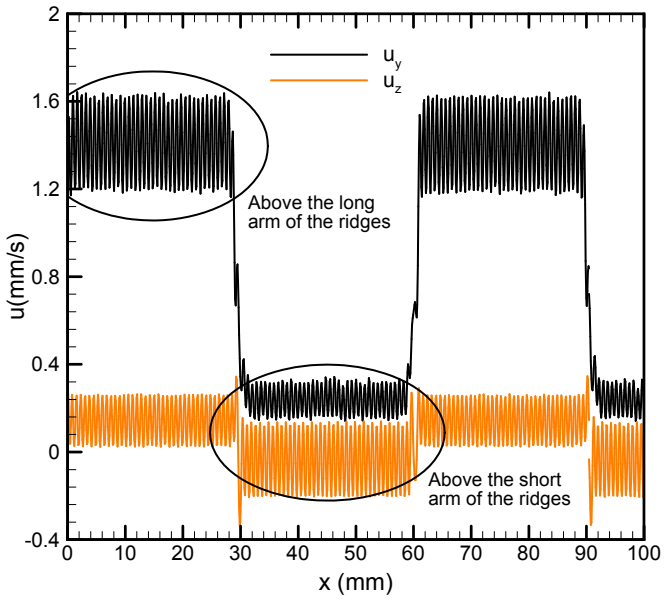

Fig. 3. Variations of the y and z components of the velocity vector along the microchannel at y = 180 μm and z = 750 μm.

constrained within the microchannels by three solid walls (a bottom and two side walls) and a hydrophobic nanofibrous membrane on the top. The membrane used in this test has a nominal pore size of 1 μm and is 80% porous. A perforated SS (stainless steel) plate with a pore size of 1.2 mm, a thickness of 0.5 mm, and an open area of 63% is used to support and secure the membrane on the microchannels. The solution microchannels are 500-μm-deep, 1-mm-wide and 195-mm-long. The water vapor generated in the evaporator flows through the membrane and is subsequently absorbed by the strong LiBr solution. To cool the solution, microchannels are machined on the backside of the brass plate (not shown). The height and width of the water channels are 0.4 mm and 4 mm, respectively. The cooling water from a chiller is pumped through the microchannels.

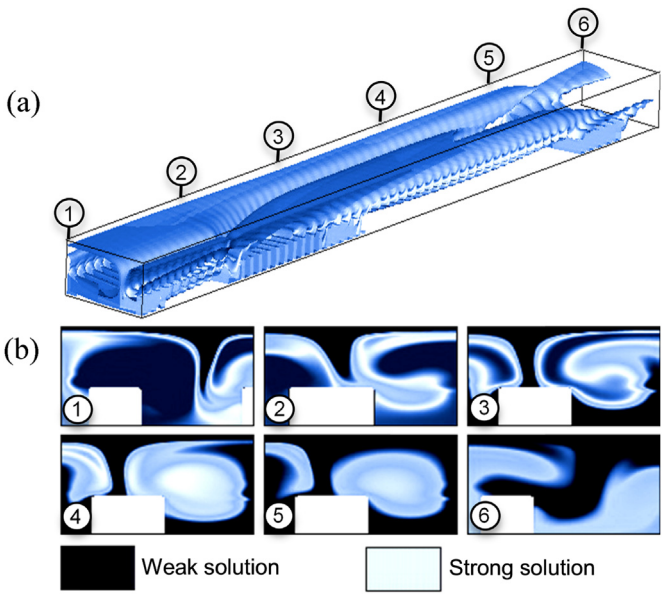

Fig. 4. (a) A 3D view of iso-concentration surfaces and (b) flow cross-sectional views showing the solution mixing process.

At the microchannels floor, the ridges are machined as per the dimensions shown in Fig. 5. As mentioned earlier, the dimensions are determined through an optimization process discussed in Bigham et al. [22]. As explained by Bigham et al. [22], the ridges direction (or pattern) is changed after a certain number of ridges (i.e. 30 in this case) because alternating between the two wall patterns continuously brings concentrated solution from the middle of vortices to the vapor–liquid interface.

3.2. Experimental setup

The studies are performed on a model membrane-based ARS. Fig. 6 shows a schematic of the experimental loop, which consists of a LiBr solution line and a refrigerant (water) line. The solution line consists of an absorber, desorber, pump, filter, solution reservoir, Coriolis mass flow meter, and two solution heat exchangers. The water line consists of an evaporator, condenser, Coriolis mass flow meter, and a water reservoir. In the solution line, a micro gear pump (HNP Mikrosysteme, Germany) drives the weak LiBr solution to a Coriolis mass flow meter (Bronkhorst USA) and then through a solution heat exchanger where the solution is preheated to a desired temperature before entering the desorber. In the desorber, the weak LiBr solution is heated by a thin film heater (Omega Engineering, CT) to desorb water. The desorbed water vapor flows to a condenser and the strong LiBr solution leaves the desorber and flows through a heat exchanger where it is cooled to a preset temperature before it enters the absorber. The condensed water leaves the condenser and flows through a Coriolis mass flow meter (Micro Motion, Inc.) to the evaporator where it is vaporized and supplied back to the absorber. The strong solution flows through the absorber and absorbs the water vapor generated in the evaporator. The weak solution leaving the absorber flows through a filter and is pumped back to the solution pre-heater and then the desorber to complete the cycle.

To control the inlet temperature of the absorber and desorber, the solution flows through the heat exchangers where it is cooled or heated using TEC (thermoelectric cooling/heating) units. A similar arrangement is implemented for the condenser heat exchanger. The desorber and evaporator heat exchangers are heated by flexible heaters. The experimental loop is also equipped with two small reservoirs with sight glass to monitor the liquid in the solution and water lines. These reservoirs also serve as compensation chambers and assist in proper charging of the loop. Three pressure transducers with a range of 0–10 kPa are installed to monitor absorber pressure conditions. Two of the transducers measure the LiBr solution flow pressure at the absorber inlet and outlet. The third transducer measures the vapor pressure (P_v) at the absorber inlet. The data measured by pressure transducers, thermocouples, and mass flow meters are recorded by a data acquisition system. Further details on the experimental setup, test procedure, and uncertainty analysis are provided in Isfahani and Moghaddam [13].

The studies are conducted on effects of water vapor pressure, cooling water temperature and solution inlet temperature. Table 2 summarizes the test conditions.

3.3. Experimental uncertainty

Table 3 lists uncertainty in measurement of pressure, solution flow rate, and temperature. The accuracy of the water mass flow meter that directly measures the water absorption rate at the condenser exit is ±1%. However, due to the unsteady nature of the condensate flow, a fluctuation of up to ±5% was recorded during the experiment. The reported absorption rates are the average of the

Please cite this article in press as: Nasr Isfahani R, et al., Impact of micromixing on performance of a membrane-based absorber, Energy (2015), http://dx.doi.org/10.1016/j.energy.2015.08.006

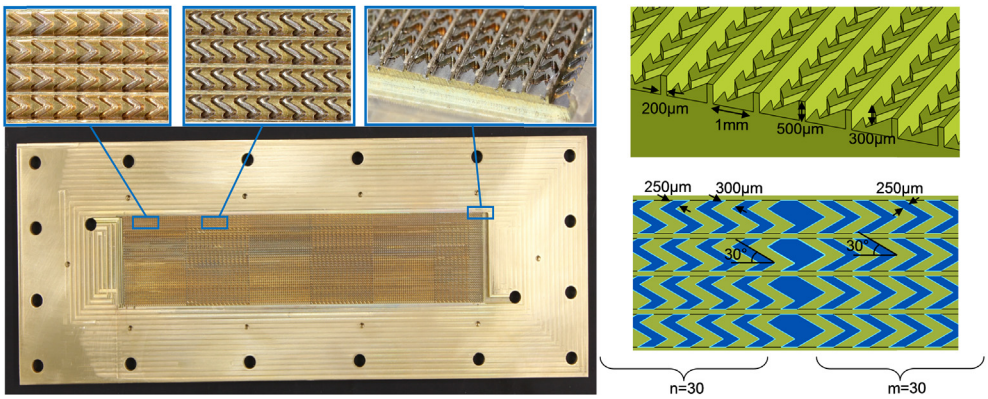

Fig. 5. Absorber heat exchanger.

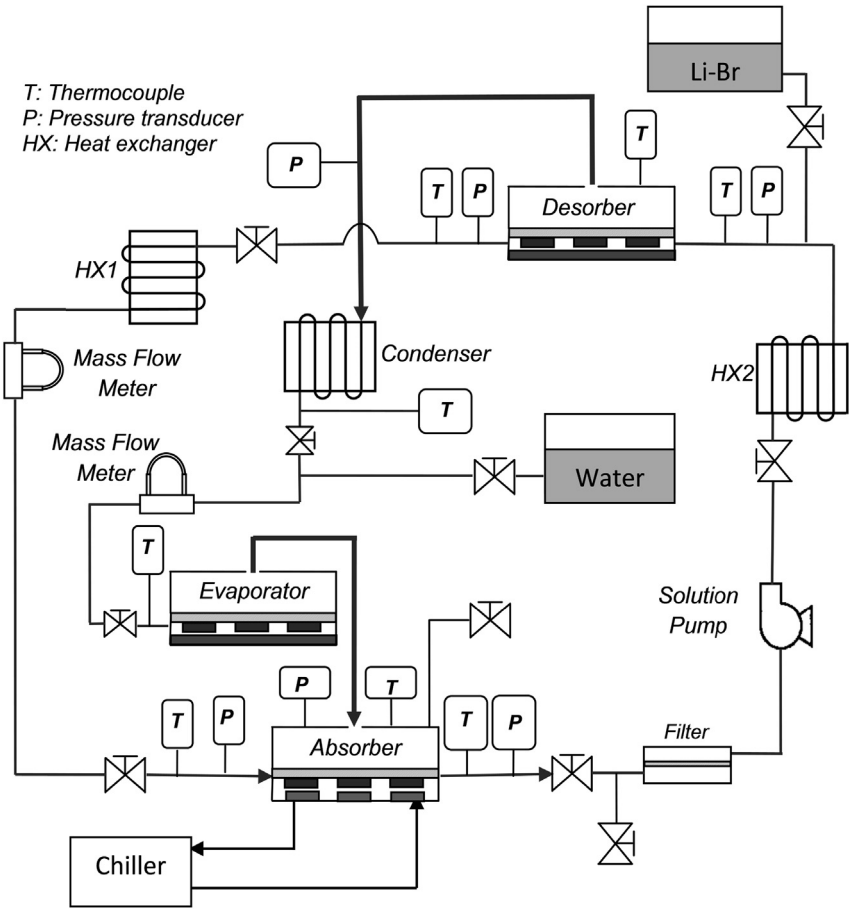

Fig. 6. Schematic of the experimental membrane-based ARS.

Table 2
Input values for parametric studies.

Parameter	Nominal	Range
Solution flow rate ($\dot{m}_{sol}$)	2.5 kg/hr	–
Cooling water inlet temperature ($T_{cw,in}$)	25 °C	25–35 °C
Solution inlet temperature ($T_{sol,in}$)	25 °C	31–43 °C
Water vapor pressure (P_v)	1.10 kPa	0.80–1.60 kPa
Inlet solution concentration (X_{in})	60 ± 1.5%	NA

Table 3
Variable uncertainties.

Variable	Uncertainty
Pressure	0.5%
Density (kg/m^3)	5 kg/m^3
Solution flow rate	0.2%
Temperature (°C)	0.3 °C
Concentration	±1%

Please cite this article in press as: Nasr Isfahani R, et al., Impact of micromixing on performance of a membrane-based absorber, Energy (2015), http://dx.doi.org/10.1016/j.energy.2015.08.006

measured values over a period of time, after the system reached a steady state.

4. Result and discussions

In the first series of tests, the effect of water vapor pressure on the absorption rate is investigated. The water vapor pressure is varied by changing the evaporator temperature. The absorption rate is measured directly by the Coriolis mass flow meter installed in the refrigerant line. Increasing the water vapor pressure increases the pressure potential between the water vapor and the LiBr solution and consequently increases the mass driving potential for the absorption process. The water vapor pressure was increased from 800 to 1600 Pa while the other test conditions were kept at the nominal values given in Table 2. Fig. 7 shows increasing of the absorption rate with the vapor pressure.

In the second series of tests, the cooling water temperature was changed from 25 to 35 °C while the other test conditions were kept constant at the nominal conditions listed in Table 2. Changing the cooling water temperature changes the solution temperature and consequently the solution water vapor pressure. This variation will ultimately lead to a change in the pressure potential and absorption rate. As shown in Fig. 8, the absorption rate decreases linearly with the cooling water temperature.

As mentioned earlier, the driving force for the absorption process is the pressure potential between the vapor and the LiBr solution. Therefore, any comparison of the absorption rates should be conducted at the same pressure potential. Fig. 9 shows the absorption rates presented in Figs. 7 and 8 as a function of the corresponding pressure potential ($P_v - P_{s,w}$). The solution water vapor pressure used in the calculation is the average of the absorber inlet and exit solution pressures. Fig. 9 also shows the results obtained in the falling film absorption studies and our previous membrane-based studies. The literature data are collected at different operating conditions (i.e. solution inlet temperature and concentration, vapor pressure, and solution flow rate). However, as mentioned earlier, since the data is plotted against the pressure potential, the differences in temperature, concentration and vapor pressure conditions are filtered out.

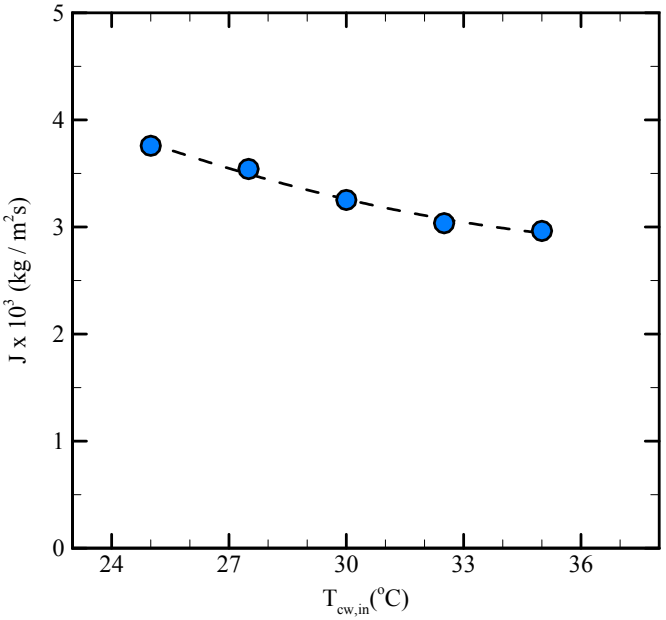

Fig. 8. Variation of absorption rate as a function of cooling water inlet temperature.

To calculate the pressure potential for the test results reported by Medrano et al. [37], Miller and Keyhani [4] and Yoon et al. [10], the solution exit temperature was assumed (since it was not reported) to be equal to the cooling water exit temperature. The results clearly suggest that the absorption rate of the 500-micron-thick solution film with herringbone ridges is as high as the absorption rate of a 100-micron-thick solution film at the operating conditions of an actual absorber (i.e. $P_v - P_{s,w} = 0.5 \sim 0.6$ kPa corresponding to an evaporator temperature of about 5 °C and a solution average concentration of 57%). The high absorption rate achieved stems from the mixing effect of vortices generated in the flow field. As mentioned in the absorber design section, the presence of ridges along with direction alteration sets up a churning motion in the

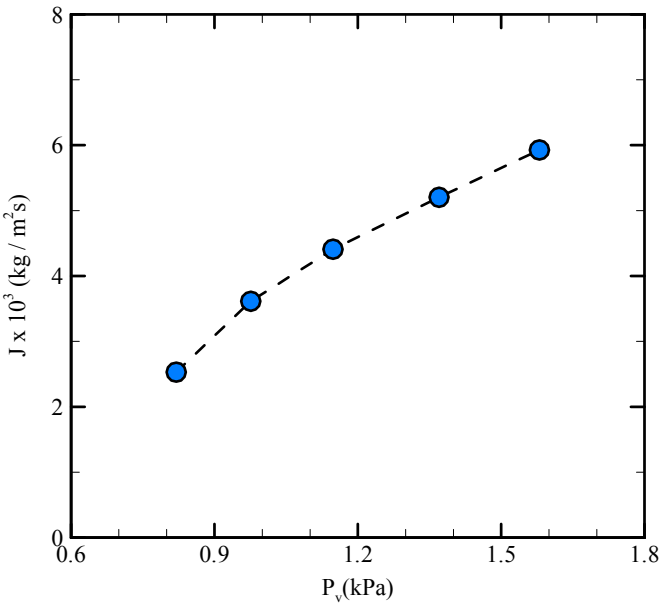

Fig. 7. Variation of absorption rate as a function of water vapor pressure.

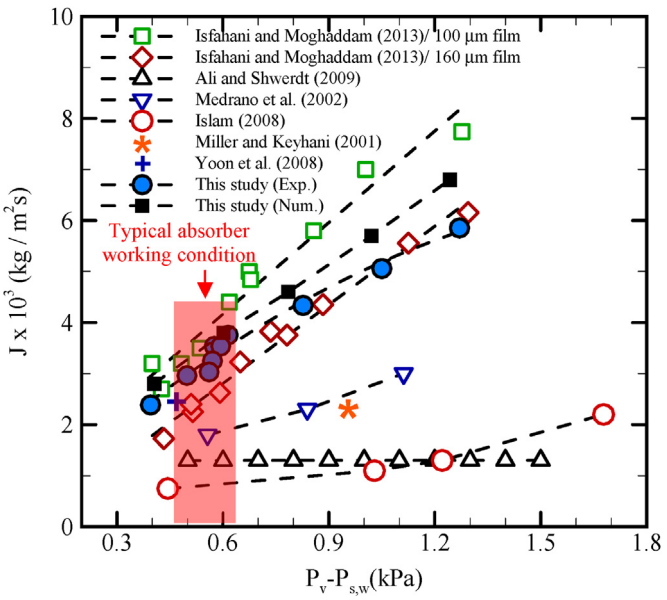

Fig. 9. Variation of absorption rate as a function of water vapor pressure potential.

Please cite this article in press as: Nasr Isfahani R, et al., Impact of micromixing on performance of a membrane-based absorber, Energy (2015), http://dx.doi.org/10.1016/j.energy.2015.08.006

bulk fluid that continuously brings concentrated solution from the bottom of the flow channel to the membrane-solution interface and carries away the weak (i.e. water-rich) solution from the absorption zone to be subsequently mixed with the bulk flow.

As mentioned earlier, in the present study absorption rates as high as that of a 100-micron-thick solution film are achieved at typical operating conditions of an absorber. The practical significance of this result becomes more apparent through a comparison of the solution pressure drop in both cases. Fig. 10 shows the pressure drop of the 500-micron-thick solution film with micromixing and that of a 100-micron-thick solution film. The results suggest a reduction of about two orders of magnitude in the pressure drop in the new approach. This observation is consistent with the laminar flow theory, as discussed earlier.

To further characterize our absorber, the significance of the membrane resistance and its contribution to the overall mass transfer resistance is investigated and the results are provided in Fig. 11. The membrane pressure drop is separately measured using a test setup discussed in Isfahani et al. [15]. Fig. 11 compares the membrane pressure drop, $P_v - P_i$ (P_i is pressure at the membrane-solution interface), with the overall pressure potential ($P_v - P_{s,w}$). The comparison suggests that the membrane mass transfer resistance is not dominant (only 10–15% of the total pressure drop) in the arrangement implemented in this study. The dominant resistance here is mass transfer through the solution ($P_i - P_{s,w}$).

Finally, the impact of solution inlet temperature on the absorption rate was studied. The results are presented in Fig. 12. The absorption rate slightly declines as the solution inlet temperature is increased. This decline in absorption rate is due to an increase in the solution water pressure that results in reduction of the pressure potential driving the absorption process. However, the high heat transfer coefficient associated with the microchannel flow results in rapid cooling of the solution flow shortly after it enters the absorber channels. Hence, the absorption process is found to be less sensitive to the solution inlet temperature, as compared to the other parametric variations presented earlier.

5. Conclusion

The effect of wall microstructures on the absorption characteristics of a membrane-based absorber has been investigated. Our results show that the absorption rate can be significantly enhanced compared to the conventional falling film absorbers when carefully designed microstructures are implemented on the flow channel wall. As elucidated in Ref. [22], implementing microstructures on flow channel wall induces a secondary flow of vortical nature within the channel bulk flow that leads to a perpetual supply of fresh absorbent into the absorption zone (i.e. near the solution-membrane interface). Consequently, in the present study, absorption rates comparable to those of membrane-based absorber employing much thinner solution films could be achieved, but at a much lower solution pressure drop. A parametric study was also carried out to examine the effect of the main variables of the ARS on the absorption rate.

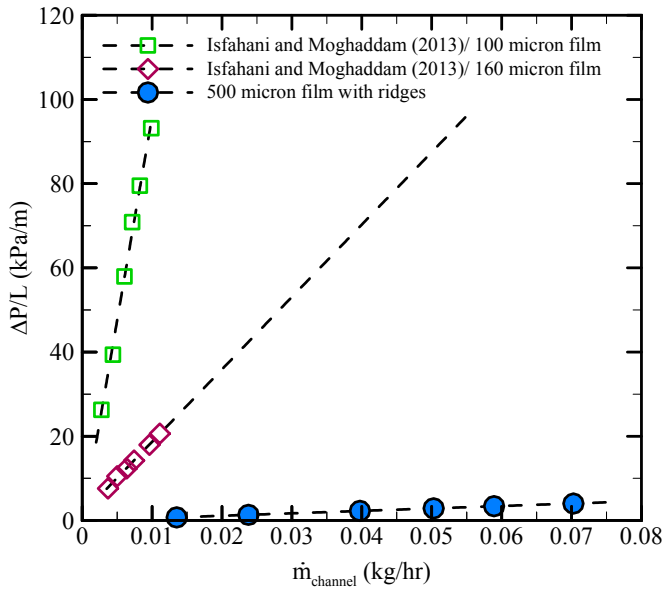

Fig. 10. Solution pressure drop as a function of flow rate.

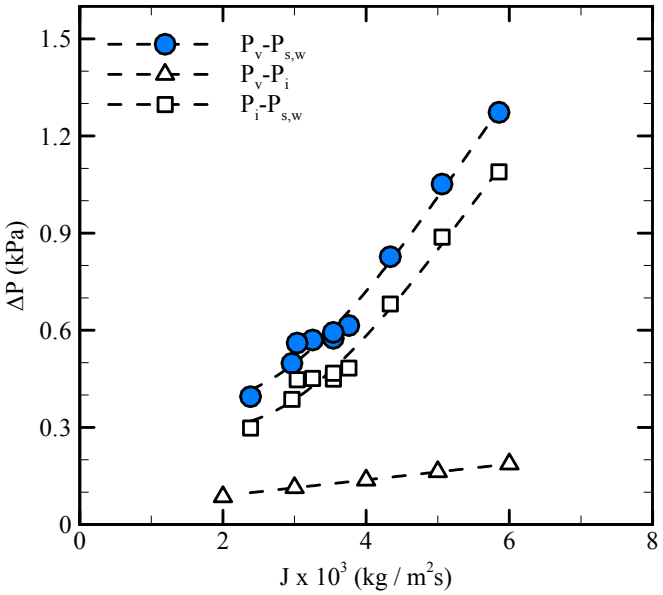

Fig. 11. Comparison between membrane and solution resistances.

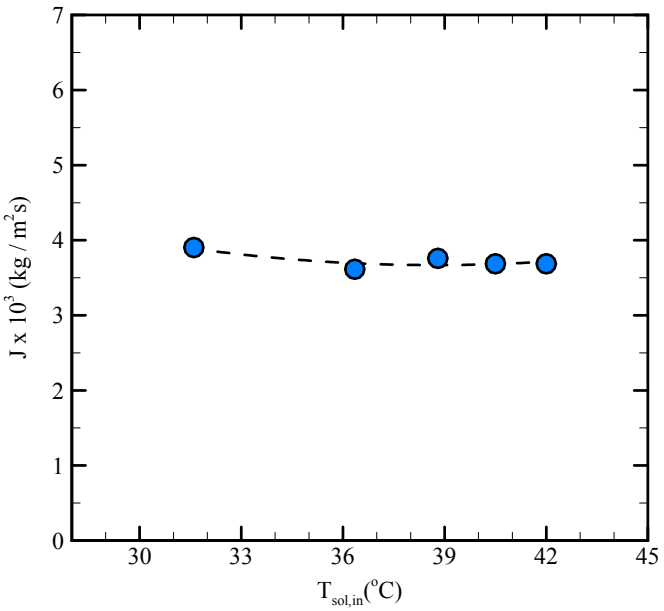

Fig. 12. Variation of absorption rate as a function of solution inlet temperature.

Please cite this article in press as: Nasr Isfahani R, et al., Impact of micromixing on performance of a membrane-based absorber, Energy (2015), http://dx.doi.org/10.1016/j.energy.2015.08.006

Acknowledgments

This study was funded by a grant from the Advanced Research Projects Agency - Energy (ARPA-E) under contract DE-AR0000133.

References

[1] Asfand F, Bourouis M. A review of membrane contactors applied in absorption refrigeration systems. Renew Sustain Energy Rev 2015;45:173–91.
[2] Islam R, Wijeysundera NE, Ho JC. Evaluation of heat and mass transfer coefficients for falling-films on tubular absorbers. Int J Refrig 2003;26:197–204.
[3] Yoon J, Kwon O, Moon C. Experimental investigation of heat and mass transfer in absorber with enhanced tubes. KSME Int J 1999;13:640–6.
[4] Miller WA, Keyhani M. The correlation of simultaneous heat and mass transfer experimental data for aqueous lithium bromide vertical falling film absorption. J Sol Energy Eng 2001;123:30. http://dx.doi.org/10.1115/1.1349550.
[5] Matsuda A, Choi KH, Hada K, Kawamura T. Effect of pressure and concentration on performance of a vertical falling-film type of absorber and generator using lithium bromide aqueous solutions. Int J Refrig 1994;17:538–42.
[6] Choudhury SK, Hisajima D, Ohuchi T, Nishiguchi A, Fukushima T, Sakaguchi S. Absorption of vapors into liquid films flowing over cooled horizontal tubes. ASHRAE Trans Res 1993;99:81–9.
[7] Jeong S, Garimella S. Falling-film and droplet mode heat and mass transfer in a horizontal tube LiBr/water absorber. Int J Heat Mass Transf 2002;45:1445–58. http://dx.doi.org/10.1016/S0017-9310(01)00262-9.
[8] Sultana P, Wijeysundera NE, Ho JC, Yap C. Modeling of horizontal tube-bundle absorbers of absorption cooling systems. Int J Refrig 2007;30:709–23. http://dx.doi.org/10.1016/j.ijrefrig.2006.09.010.
[9] Raisul Islam M, Wijeysundera N, Ho J. Performance study of a falling-film absorber with a film-inverting configuration. Int J Refrig 2003;26:909–17. http://dx.doi.org/10.1016/S0140-7007(03)00078-1.
[10] Yoon J-I, Kwon O-K, Bansal PK, Moon C-G, Lee H-S. Heat and mass transfer characteristics of a small helical absorber. Appl Therm Eng 2006;26:186–92. http://dx.doi.org/10.1016/j.applthermaleng.2005.05.009.
[11] Ali AHH. Design of a compact absorber with a hydrophobic membrane contactor at the liquid–vapor interface for lithium bromide–water absorption chillers. Appl Energy 2010;87:1112–21. http://dx.doi.org/10.1016/j.apenergy.2009.05.018.
[12] Ali AHH, Schwerdt P. Characteristics of the membrane utilized in a compact absorber for lithium bromide–water absorption chillers. Int J Refrig 2009;32:1886–96. http://dx.doi.org/10.1016/j.ijrefrig.2009.07.009.
[13] Isfahani RN, Moghaddam S. Absorption characteristics of lithium bromide (LiBr) solution constrained by superhydrophobic nanofibrous structures. Int J Heat Mass Transf 2013;63:82–90.
[14] Riffat SB, Wu S, Bol B. Pervaporation membrane process for vapor absorption system. Int J Refrig 2004;27:604–11.
[15] Nasr Isfahani R, Sampath K, Moghaddam S. Nanofibrous membrane-based absorption refrigeration system. Int J Refrig 2013;36:2297–307.
[16] Thorud JD, Liburdy JA, Pence DV. Microchannel membrane separation applied to confined thin film desorption. Exp Therm Fluid Sci 2006;30:713–23. http://dx.doi.org/10.1016/j.expthermflusci.2006.03.001.
[17] Isfahani RN, Fazeli A, Bigham S, Moghaddam S. Physics of lithium bromide (LiBr) solution dewatering through vapor venting membranes. Int J Multiph Flow 2014;58:27–38.
[18] Bigham S, Nasr Isfahani R, Moghaddam S. Direct molecular diffusion and micro-mixing for rapid dewatering of LiBr solution. Appl Therm Eng 2014;64:371–5.
[19] Yu D, Chung J, Moghaddam S. Parametric study of water vapor absorption into a constrained thin film of lithium bromide solution. Int J Heat Mass Transf 2012;55:5687–95.
[20] Nasr Isfahani R, Moghaddam S. Experimental study of water vapor absorption into lithium bromide (LiBr) solution constrained by superhydrophobic porous membranes. In: ASME 2013 Heat Transf. Summer Conf., Minneapolis, Minnesota, USA; 2013.
[21] Drost K, Liburdy J, Paul B, Peterson R. Enhancement of heat and mass transfer in mechanically constrained ultra thin films. DOE Final Report No. FC36–01GO11049. 2005. http://www.osti.gov/scitech/biblio/861948-KToumV/.
[22] Bigham S, Yu D, Chugh D, Moghaddam S. Moving beyond the limits of mass transport in liquid absorbent microfilms through the implementation of surface-induced vortices. Energy 2014;65:621–30.
[23] Sudarsan AP, Ugaz VM. Multivortex micromixing. Proc Natl Acad Sci U S A 2006;103:7228–33. http://dx.doi.org/10.1073/pnas.0507976103.
[24] Ottino JM, Wiggins S. Designing optimal micromixers. Science 2004;305:485–6. http://dx.doi.org/10.1126/science.1099343.
[25] Xi C, Marks DL, Parikh DS, Raskin L, Boppart SA. Structural and functional imaging of 3D microfluidic mixers using optical coherence tomography. Proc Natl Acad Sci U S A 2004;101:7516–21. http://dx.doi.org/10.1073/pnas.0402433101.
[26] Stroock AD, Dertinger SKW, Ajdari A, Mezic I, Stone HA, Whitesides GM. Chaotic mixer for microchannels. Science 2002;295:647–51. http://dx.doi.org/10.1126/science.1066238.
[27] Yu D, Ladd AJC. A numerical simulation method for dissolution in porous and fractured media. J Comput Phys 2010;229:6450–65. http://dx.doi.org/10.1016/j.jcp.2010.05.005.
[28] He X, Luo L. A priori derivation of the lattice Boltzmann equation. Phys Rev E 1997;55:6333–6.
[29] Mason EA, Malinauskas AP. Gas transport in porous media: the dusty-gas model. New York: Elsevier Scientific Pub; 1983.
[30] Kyung I, Herold KE, Kang YT. Model for absorption of water vapor into aqueous LiBr flowing over a horizontal smooth tube. Int J Refrig 2007;30:591–600. http://dx.doi.org/10.1016/j.ijrefrig.2006.11.001.
[31] Bo S, Ma X, Lan Z, Chen J, Chen H. Numerical simulation on the falling film absorption process in a counter-flow absorber. Chem Eng J 2010;156:607–12. http://dx.doi.org/10.1016/j.cej.2009.04.066.
[32] Papaefthimiou VD, Koronaki IP, Karampinos DC, Rogdakis ED. A novel approach for modelling LiBr–H_2O falling film absorption on cooled horizontal bundle of tubes. Int J Refrig 2012;35:1115–22. http://dx.doi.org/10.1016/j.ijrefrig.2012.01.015.
[33] McNeely LA. Thermodynamic properties of aqueous solutions of lithium bromide. ASHRAE Trans 1979;85:413–34.
[34] McNamara G, Zanetti G. Use of the Boltzmann equation to simulate lattice-gas automata. Phys Rev Lett 1988;61:2332–5.
[35] Beskok A, Karniadakis GE. A model for flows in channels, pipes, and ducts at micro and nano scales. Microscale Thermophys Eng 1999;3:43–77.
[36] Sundararajan P, Stroock AD. Transport phenomena in chaotic laminar flows. Annu Rev Chem Biomol Eng 2012;3:473–96.
[37] Medrano M, Bourouis M, Coronas A. Absorption of water vapour in the falling film of water–lithium bromide inside a vertical tube at air-cooling thermal conditions. Int J Therm Sci 2002;41:891–8. http://dx.doi.org/10.1016/S1290-0729(02)01383-2.

Please cite this article in press as: Nasr Isfahani R, et al., Impact of micromixing on performance of a membrane-based absorber, Energy (2015), http://dx.doi.org/10.1016/j.energy.2015.08.006